

# Analysis of current–voltage characteristics for Langmuir probes immersed in an ion beam

Cite as: Rev. Sci. Instrum. **91**, 023504 (2020); <https://doi.org/10.1063/1.5128669>

Submitted: 20 September 2019 . Accepted: 13 January 2020 . Published Online: 05 February 2020

 E. Sartori, V. Candeloro, and  G. Serianni

## COLLECTIONS

Paper published as part of the special topic on [Proceedings of the 18th International Conference on Ion Sources](#)



View Online



Export Citation



CrossMark

## ARTICLES YOU MAY BE INTERESTED IN

[Overview of high intensity ion source development in the past 20 years at IMP](#)



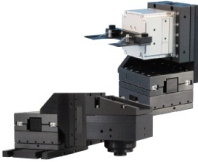
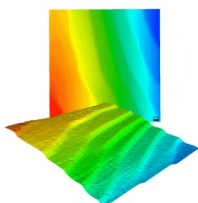
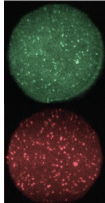
Review of Scientific Instruments **91**, 023310 (2020); <https://doi.org/10.1063/1.5129399>

[Study of correlation between plasma parameter and beam optics](#)

Review of Scientific Instruments **91**, 023503 (2020); <https://doi.org/10.1063/1.5131102>

[First operation in SPIDER and the path to complete MITICA](#)

Review of Scientific Instruments **91**, 023510 (2020); <https://doi.org/10.1063/1.5133076>

 <b>MCL</b> MAD CITY LABS INC. <a href="http://www.madcitylabs.com">www.madcitylabs.com</a>	<p>Nanopositioning Systems</p> 	<p>Modular Motion Control</p> 	<p>AFM and NSOM Instruments</p> 	<p>Single Molecule Microscopes</p> 
---	--	--	---	--

# Analysis of current–voltage characteristics for Langmuir probes immersed in an ion beam

Cite as: Rev. Sci. Instrum. 91, 023504 (2020); doi: 10.1063/1.5128669

Submitted: 20 September 2019 • Accepted: 13 January 2020 •

Published Online: 5 February 2020



View Online



Export Citation



CrossMark

E. Sartori,<sup>1,2</sup>  V. Candeloro,<sup>2</sup> and G. Serianni<sup>1,a)</sup> 

## AFFILIATIONS

<sup>1</sup>Consorzio RFX, Corso Stati Uniti 4, 35127 Padova (PD), Italy

<sup>2</sup>Università degli Studi di Padova, Via 8 Febbraio 2, I-35122 Padova (PD), Italy

**Note:** Contributed paper, published as part of the Proceedings of the 18th International Conference on Ion Sources, Lanzhou, China, September 2019.

<sup>a)</sup>Author to whom correspondence should be addressed: [gianluigi.serianni@igi.cnr.it](mailto:gianluigi.serianni@igi.cnr.it)

## ABSTRACT

Movable electrical probes were used to diagnose the beam flux profile and potential of ion beams since the early 1960s. Experimental measurements of beam plasmas can provide essential data related to the space charge neutralization, but the current–voltage characteristics obtained from such electrical probes are dominated by beam ion impact and ion-induced secondary emission. In this work, we present an analysis of the Langmuir characteristics obtained in a negative ion beam. We identify and discuss separately the contributions to the collected current given by secondary plasma ions and electrons, stripped electrons, beam ions, and ion-induced secondary electron emission. We present the beam plasma parameters obtained at different beam energies in NIO1.

Published under license by AIP Publishing. <https://doi.org/10.1063/1.5128669>

## I. INTRODUCTION

Neutral beam injectors are one of the most applied techniques for fusion plasma heating. Fast neutrals are obtained through charge exchange and neutralization of the precursor ion beams colliding with background gas. The precursor beam is usually made of  $H^+$  or  $H^-$  ions<sup>1</sup> chosen according to the target energy of the neutral beam, as the neutralization efficiency for  $H^+$  beams at 100 kV drops below 20%. As charged particles are subject to Coulomb forces, self-field effects affect the transport of the ion beams, in the absence of external electromagnetic fields, so that the beam space charge produces a defocusing effect. The equation for the beam radius  $r_m(z)$  in drift space  $z$  is commonly written<sup>2</sup> in the form  $r_m'' = \beta/r_m$ , showing the effect of the generalized perveance  $\beta$  on the divergence growth of a beamlet. The generalized perveance  $\beta$  includes the beamlet current  $I$  and the beam ion velocity  $v$  and mass  $m$ ,

$$\beta = \frac{qI(1 - f_e)}{2\pi\epsilon_0mv^3},$$

with  $\epsilon_0$  being the vacuum permittivity and  $q$  the ion charge. As the propagating beam causes collisional ionization of the low-density background gas, secondary charges with opposite sign are trapped in

the beam, thus partially neutralizing the beam space charge. In the previous equation, the charge-compensation factor  $f_e$  (ratio between the charge density of particles of opposite polarity and the charge density of the beam ions) is used to account for this effect. Experimental and theoretical studies on ion beam plasma were performed since the early 1960s,<sup>3–6</sup> also focusing on minimizing the divergence growth in the low-energy transport region by space charge compensation in the presence of background gas. Some studies were performed specifically on  $H^-$  beams.<sup>7,8</sup> Experimental data about the space charge compensation are lacking in the case of multi-beamlet negative ion beams for fusion. In this paper, we present the analysis of the current–voltage (CV) characteristics obtained from a Langmuir probe immersed in a negative ion beam. The purpose of this analysis is to attempt an estimation of the properties of the secondary plasma produced by a charge-neutralized negative ion beam.

## II. METHOD TO EXTRACT BEAM PLASMA PARAMETERS

In this paper, a dataset consisting of 11 CV characteristics is used. The data are obtained in the NIO1 experiment<sup>9</sup> (Negative Ion

Optimization phase 1) using a cylindrical probe inserted in the  $H^-$  beam approximately 0.5 m downstream with respect to the accelerator. The probe tip has a diameter  $d$  of 2.4 mm and a length  $l$  of 15 mm. Different acceleration voltages were tested. The ion source is operated in pure volume production. The analytical model describes the contribution to the CV characteristics, allowing the determination of the parameters of the secondary plasma. The total current as a function of the probe voltage  $V$  is

$$I(V) = I_b(V) + I_{pi}(V) + I_{pe}(V) + I_{see}(V) + I_{se}(V), \quad (1)$$

where  $I_b$ ,  $I_{pi}$ ,  $I_{pe}$ ,  $I_{se}$ , and  $I_{see}$  are the currents due to beam ions, plasma ions, plasma electrons, stripped electrons, and secondary emission electrons, respectively. The formula describing each contribution changes depending on the probe potential being larger or smaller than the plasma potential,  $V_p$ .

The collected beam ion current depends on the charge state of the beam particles, which evolves along the drift space  $z$ . It can be defined as the integral over the collection surface  $A_{beam}$  of the negative and positive ion current densities  $j_{H-}$  and  $j_{H+}$ ,

$$I_b = \int_{A_{beam}} (j_{H-} - j_{H+}) d\Sigma. \quad (2)$$

For the beam ions, we assume that  $A_{beam}$  is not affected by orbital effects, and thus,  $A_{beam} = 2al$  depends only on the probe radius  $a$  and on the exposed length of the probe  $l$ . Both  $j_{H-}$  and  $j_{H+}$  are defined as positive quantities, and if the contribution to the collected current expected for positive ions is very small, the latter can be neglected for our application.

For  $V < V_p$ , positive plasma ions reads

$$I_{pi} = -qS_{eff}^{pi} n_{pi,s} u_B^*, \quad (3)$$

where  $n_{i,s}$  is the positive ion density at the sheath edge,  $s$ , whereas  $u_B^*$  is a modified Bohm velocity and the probe collection surface  $S_{eff}^{pi}$  is defined as in the [Appendix](#) (see also the discussion in Sec. III). If  $V > V_p$ , the collection area for positive plasma ions is equal to the geometrical surface of the probe  $A_{probe} = 2\pi al + \pi a^2$ , and thus,

$$I_{pi} = -qA_{probe} n_{pi,s} u_B^* \exp\left(-\frac{V - V_p}{T_i}\right), \quad (4)$$

with the Boltzmann factor including the ion temperature  $T_i$  (in eV).

For  $V < V_p$ , negative charges are repelled from the probe and the plasma electron (PE) current is given via Boltzmann relation,

$$I_{pe} = \frac{1}{4} q n_{pe,s} A_{probe} \bar{v} \exp\left(\frac{V - V_p}{T_e}\right), \quad (5)$$

with average speed  $\bar{v} = \sqrt{8qT_e/\pi m_e}$ . For  $V > V_p$ ,  $I_{pe}$  becomes

$$I_{pe} = \frac{1}{4} q n_{pe,s} \bar{v} S_{eff}^{pe}, \quad (6)$$

where  $S_{eff}^{pe} = 2\pi b_{pe} l + 2\pi b_{pe}^2$  is the effective collection area and  $b_{pe}$  is the impact parameter obtained from the OML (Orbital Motion Limited) theory.<sup>10</sup>

The secondary electron emission (SEE) current depends on the effective coefficient for fast atom impact, defined as  $\gamma_{see}^{eff}(\theta) = \sec(\theta)\gamma_{see}$ , with  $\theta$  being the incidence angle of beam ions over the cylindrical surface of the probe. For  $V < V_p$ , the SEE current is seen by the probe as an apparent positive ion current,

$$I_{see,-} = -\left(\frac{\pi}{2}\gamma_{see} I_{H0} + \left(\frac{\pi}{2}\gamma_{see} + 1\right) I_{H-}\right), \quad (7)$$

where  $\pi/2$  results from the integration over  $\theta$  and the extra electron is assumed to be lost by the negative ion during the impact and to be emitted from the surface.  $I_{H-}$  and  $I_{H0}$  are positive quantities, respectively, corresponding to the negative ion and to the fast atom beam currents intercepted by the probe ( $I_{H0}$  is expressed as an equivalent current). If  $V > V_p$ , the probe holds back the secondary electrons;<sup>11</sup> for simplicity, we assumed a Maxwellian distribution for the energy of secondary electrons at a temperature  $T_{see}$  (in eV),

$$I_{see} = I_{see,-} \exp\left(-\frac{V - V_p}{T_{see}}\right) \cdot \sqrt{1 + \frac{V - V_p}{T_{see}}}. \quad (8)$$

The contribution from single and double electron stripping processes is proportional to the negative ion beam current at the probe, which we indicate by a proportionality coefficient  $\alpha_{se}$ ,

$$I_{se} = \alpha_{se} I_{H-} \frac{S_{eff}^{se}}{A_{beam}}. \quad (9)$$

The effective collecting area for stripped electrons is defined as  $S_{eff}^{se} = 2b_{se}l$ , with impact parameter  $b_{se}$  given by OML theory. The initial stripped electron velocity is  $v_{se} = \sqrt{2E_{beam}/m_e}$ .

The density of negative and positive beam ions at  $s$  reads

$$n_{H\pm} = \frac{I_{H\pm}}{qA_{beam}} \sqrt{\frac{m_{H\pm}}{2e}} U_b^{-1/2}. \quad (10)$$

The density of the secondary emission electrons at  $s$  reads

$$n_{see,s} = -\frac{I_{see}}{qA_{beam}} \sqrt{\frac{m_e}{2e}} (U_{see} + V_s)^{-1/2}, \quad (11)$$

where  $U_{see} = T_{see}/2$  is the secondary emission initial energy and  $V_s$  is the potential drop at  $s$ . The stripped electron density at  $s$  is

$$n_{se,s} = \frac{\alpha_{se}}{q} I_{H-} \frac{S_{eff}^{se}}{A_{beam}} \sqrt{\frac{m_e}{2e}} (U_{se} + V_s)^{-1/2}, \quad (12)$$

where  $U_{se} = U_b m_e/m_{H-}$  is the energy of the stripped electrons, assuming that they are generated with the same velocity as the beam particles. The electron density at the sheath edge is correlated with the total beam density by the overcompensation fraction,

$$K = \frac{n_{pe,s}}{n_{beam}}. \quad (13)$$

In electronegative plasmas, the negative ion fraction is commonly indicated as  $\alpha = n_{ni,s}/n_{pe,s}$ , where  $n_{ni,s}$  is the negative ion density. In our description, the overcompensation degree  $K$  is qualitatively similar to the inverse of  $\alpha$ , even though it directly relates to space charge compensation. In fact, for our experimental

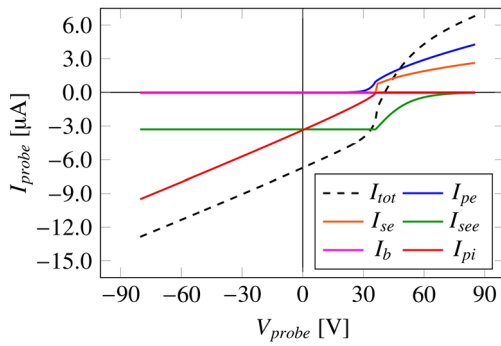


**FIG. 1.** Example of CV characteristics composed by summing up the contributions from beam ions, secondary plasma ions and electrons, secondary emission electrons, and stripped electrons.

results, complete space charge compensation was assumed. Consequently, the positive ion density will be equal to or greater than the total density of negative charges (beam ions and secondary electrons) with the possibility of overcompensation (producing a slightly focusing effect on the beam). Quasi-neutrality is assumed at the plasma sheath edge so that the density of positive plasma ions at  $s$  can be obtained as

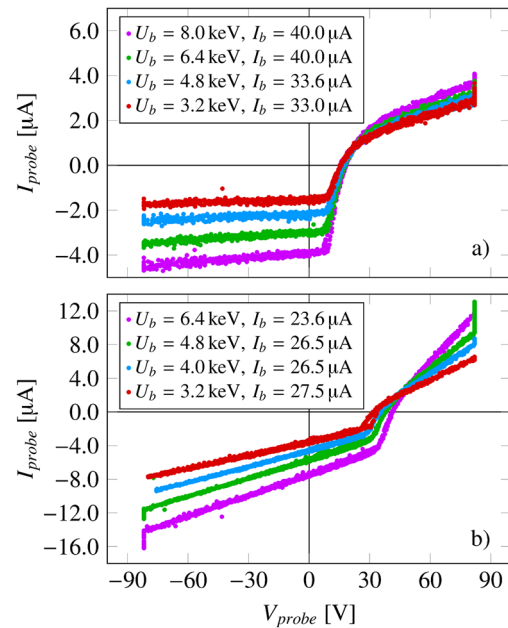
$$n_{pi,s} = n_{pe,s} + n_{se,s} + n_{see,s} + (n_{H-} - n_{H+}). \quad (14)$$

The fit function for the CV characteristics, composed of all aforementioned contributions, has, therefore, the following independent parameters: overcompensation degree  $K$ , plasma potential  $V_p$ , electron temperature  $T_e$ , secondary emission electron temperature  $T_{see}$ , secondary emission coefficient  $\gamma_{see}$ , and stripping coefficient  $\alpha_{se}$ . A qualitative example of the five current contributions is presented in Fig. 1, also indicating the resulting CV characteristic curve.

### III. RESULTS AND DISCUSSION

The experimental CV characteristics obtained in NIO1 for different beam energies are shown in Fig. 2 for vessel pressures of 30 mPa and 375 mPa; the evolution of the beam species for these conditions was estimated earlier.<sup>12</sup> An effective mass of 2 amu is assumed for the positive ions<sup>13</sup> (compensated by  $H_2^+$  ions).

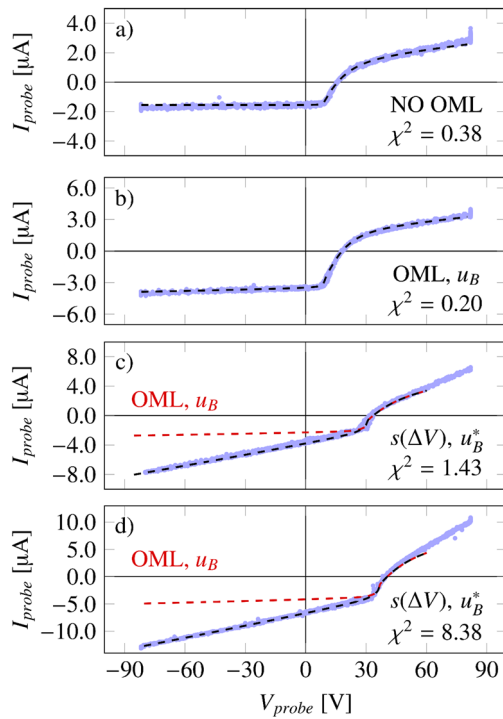
Four examples of best-fitting characteristics are given in Fig. 3 for the low-pressure [Figs. 3(a) and 3(b)] and the high-pressure regimes [Figs. 3(c) and 3(d)]. In Fig. 3(a), the variation of the effective collecting area  $S_{eff}^{pi}$  for the collection of positive ions was neglected, given the small dependence of the ion branch of the characteristics on the applied probe voltage  $V$ . In Fig. 3(b), the OML theory is applied to the ion branch also. In both cases, an unmodified Bohm velocity was assumed,  $u_B = \sqrt{qT_e/m_{pi}}$ . For the high-pressure regime, the OML theory underestimates the slope of the positive ion branch of the characteristics. A numerical simulation (see the Appendix) of the sheath thickness as a function of  $V - V_p$  was attempted, including the beam ions and secondary electrons, but provided a slope about ten times larger



**FIG. 2.** Raw experimental CV characteristics obtained for the case of (a) low gas pressure in the drift space (cryogenic pump turned on,  $p_{vessel} = 0.030$  Pa) and (b) high gas pressure in the drift space (cryogenic pump turned off,  $p_{vessel} = 0.375$  Pa).  $U_b$  and  $I_b$  are the beam extraction energy and current, respectively.

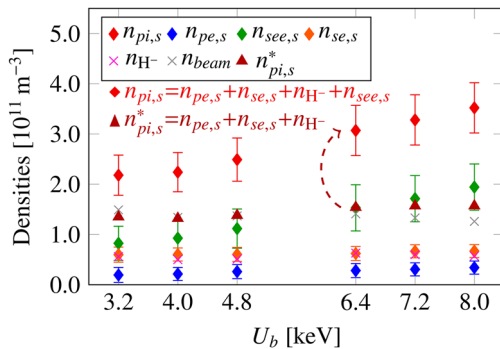
than the observed one. Therefore, in the high-pressure regime, the function  $S_{eff}^{pi}(V)$  was tuned to match the experimental slope; furthermore, a modified Bohm velocity  $u_B^*$  was introduced (see the Appendix). The  $\chi^2$  values obtained for the fitted characteristics in Fig. 3 are shown in the figure; the last two values decrease to  $\chi^2(c) = 0.52$  and  $\chi^2(d) = 0.24$  if the electron branch is neglected (i.e.,  $V \leq V_p$ ).

Figure 4 shows the secondary plasma densities obtained from the fit procedures for the low-pressure regime, compared to the total beam density  $n_{beam} = n_{H-} + n_{H0} + n_{H+}$ . The ratio  $n_{pi}/n_{beam}$  ranges between 1.5 and 3, while  $K = n_{pe,s}/n_{beam} = 0.15-0.35$  depending on the beam energy. Due to the low beam energy and relatively high-pressure, both conditions favorable to the stripping of the fast negative ions,  $n_{H-}$  is rather low and the ratio  $n_{se,s}/n_{H-}$  is close to unity. SEE gives the largest contribution to the electron density at the sheath edge: in this regard, it could be argued that the probe is strongly perturbing the beam plasma. The dashed arrow in Fig. 4 shows that  $n_{pi}$  would be halved if the SEE contribution to quasi-neutrality were neglected. However, as diffusion of secondary charges out of the beam region is dominated by the heavier positive molecular ions rather than by electrons, the measured  $n_{pi,s}$  might be a better indication for the secondary plasma density unperturbed by the probe, rather than  $n_{pe,s}$ . In our estimation, the ratio of positive ions to negative beam ion density  $n_{pi}/n_{beam}$  was found to be between 2 and 6 in this energy range and background pressure. Despite the rather strong effect of the SEE, it was possible to provide an estimate of the plasma electron temperature and the plasma potential  $V_p$



**FIG. 3.** Examples of fitted CV characteristics: (a)  $p_{\text{vessel}} = 0.030$  Pa,  $U_b = 3200$  keV; (b)  $p_{\text{vessel}} = 0.030$  Pa,  $U_b = 7200$  keV; (c)  $p_{\text{vessel}} = 0.375$  Pa,  $U_b = 3200$  keV; and (d)  $p_{\text{vessel}} = 0.375$  Pa,  $U_b = 5600$  keV. In each case, the goodness of fit ( $\chi^2$ ) is indicated, computed over the points of the dashed curve.

(Fig. 5). The beam dump was biased to 60 V during these measurements. The plasma densities obtained in the high-pressure regime are presented in Fig. 6. In the high-pressure regime, the charge state of beam particles hitting the probe does not include  $H^-$  ions any longer and the beam is mostly neutralized, with a minor presence of  $H^+$  ions. Consequently, the neutralization of the beam space charge is almost not necessary, and the beam does not contribute to the confinement of positive ions. However, the obtained positive ion



**FIG. 4.** Density of secondary plasma species obtained from the fitting procedure for the low-pressure regime.

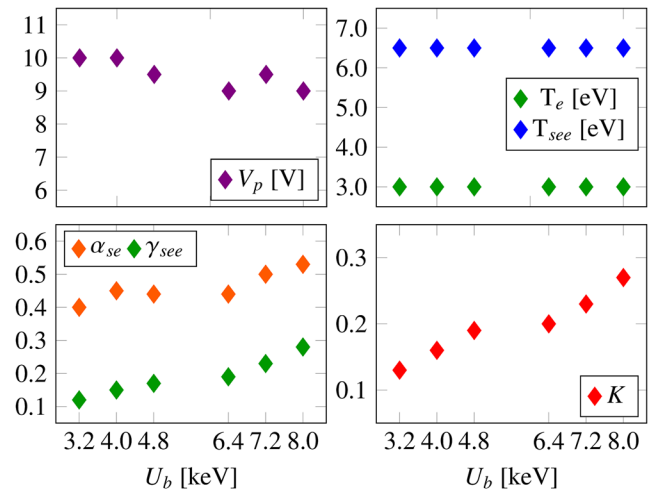


**FIG. 5.** Plasma potential  $V_p$ , electron temperature  $T_e$ , secondary electron coefficients, and overcompensation degree for the low-pressure regime. Upper limits of the average error are 0.05 for  $\gamma_{\text{see}}$ , 0.2 for both  $\alpha_{\text{se}}$  and  $K$ , 0.5 eV for  $T_e$  and  $T_{\text{see}}$ , and 0.5 V for  $V_p$ .

density is similar to the low-pressure regime, as in the latter case, the secondary plasma density is much greater than the  $n_{H^-}$  density, and the confinement of secondary charges is anyway determined by their diffusion (or, possibly, by externally applied voltages at surfaces). This applies also to the high-pressure case, where quasi-neutrality in the beam region depends on the mobility of positive ions and electrons.

In summary, the present paper describes the development of a model including all contributions to the CV curve of a Langmuir probe immersed in the beam plasma of an  $H^-$  beam. The model was applied to the low-density beam created in the NIO1 device. A simpler analysis, based on the OML theory, seems to describe, with good agreement, the experimental results at low background gas pressure. At higher pressures, a first attempt at describing the sheath expansion as a function of the applied voltage was made, to be improved

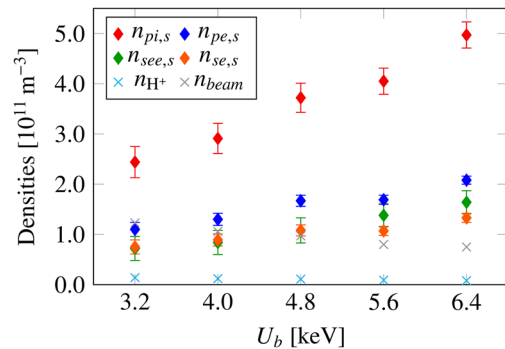


**FIG. 6.** Density of secondary plasma species obtained from the fitting procedure for the high-pressure regime.

in the future on the basis of new measurements and by comparison with other diagnostic techniques.

### ACKNOWLEDGMENTS

This work has been carried out within the framework of the EUROfusion Consortium and has received funding from the Euratom research and training programme 2014–2018 under Grant Agreement No. 633053. The views and opinions expressed herein do not necessarily reflect those of the European Commission.

### APPENDIX: SHEATH CHARACTERISTIC DIMENSION AND BOHM VELOCITY

The potential bias between the probe and the surrounding plasma causes the formation of a sheath around the probe tip. Together with the orbital effects of particle motion, this phenomenon produces an increase in the effective probe collection surface. Most of the existing theories provide a description of the sheath formation, although they do not take into account the energetic ion beams. The effective collection surface for the positive ion contribution depends on the sheath thickness<sup>14</sup>  $s(\Delta V)$ , with  $\Delta V = V - V_p$ . Similarly, to previous definitions,  $S_{eff}^{pi}$  is described as

$$S_{eff}^{pi} = 2\pi l(s(\Delta V) + a) + 2\pi(s(\Delta V) + a)^2. \quad (A1)$$

In order to obtain  $s(\Delta V)$ , we solved the following system:

$$\begin{cases} \frac{1}{r} \left( r \frac{\partial E(r)}{\partial r} \right) = \frac{q}{\epsilon_0} n_{tot} \\ \frac{1}{2} m_{pi} u_B^{*2}(r) = -q \cdot \Delta V, \end{cases} \quad (A2)$$

where the considered equations are the Gauss law and the energy conservation for the positive ions (assumed to be  $H^+$ ). The result of this computation provides the sheath characteristic dimension as a function of the plasma parameters,

$$s(\Delta V) = \lambda_{De} \sqrt{\frac{\Delta V}{T_e}} \sqrt{\frac{1 - \alpha_s \gamma_s - \alpha_s^I \gamma_s^I - \alpha_s^{II} \gamma_s^{II}}{1 + \alpha_s + \alpha_s^I + \alpha_s^{II}}}, \quad (A3)$$

with

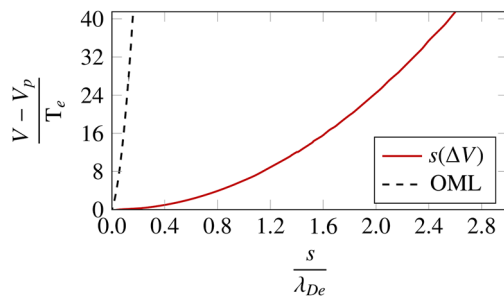


**FIG. 7.** Comparison between the OML result and numerical simulation for the sheath thickness as a function of the potential drop.

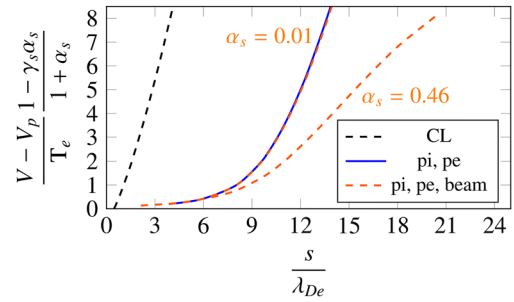


**FIG. 8.** Sheath thickness as a function of the potential drop for different values of  $\alpha_s$  compared with the Child–Langmuir expression in Cartesian coordinates. Both the secondary emission and stripping electrons contributions were neglected.

$$\alpha_s = \frac{n_{H^-}}{n_{e,s}}, \alpha_s^I = \frac{n_{see,s}}{n_{e,s}}, \alpha_s^{II} = \frac{n_{se,s}}{n_{e,s}}, \quad (A4)$$

$$\gamma_s = \frac{T_e}{2U_b}, \gamma_s^I = \frac{T_e}{2(U_{see} + V_s)}, \gamma_s^{II} = \frac{T_e}{2(U_{se} + V_s)}.$$

The normalization factor can be derived by imposing quasi-neutrality at the sheath edge and also that the derivative of the total space charge density with respect to the probe potential  $V$  is equal to zero at sheath edge.<sup>15</sup> The sheath thickness  $s(\Delta V)$  can then be expressed as a function of the plasma parameters. In addition, a modified Bohm velocity can be introduced by considering Amemiya's criteria,<sup>15</sup>

$$u_B^* = \sqrt{\frac{qT_e}{m_{pi}}} \sqrt{\frac{1 + \alpha_s + \alpha_s^I + \alpha_s^{II}}{1 - \alpha_s \gamma_s - \alpha_s^I \gamma_s^I - \alpha_s^{II} \gamma_s^{II}}}. \quad (A5)$$

Figure 7 shows the comparison between the OML theory result and the numerical simulation for  $s(\Delta V)$ . Furthermore, by this model, we were able to investigate the dependence of the sheath dimension on the energetic ion beam density. As it can be seen in Fig. 8,  $s(\Delta V)$  is larger for increasing values of  $\alpha_s$ , i.e., when the  $H^-$  density prevails on the plasma electron one. In particular, for  $\alpha_s = 0.01$ , there is a nearly complete superposition with the blue curve obtained without considering the ion beam. As a final remark, it is worth noting that the model described herein is valid until a virtual cathode starts to form in the immediate proximity of the probe.

### REFERENCES

- <sup>1</sup>S. Hemsworth *et al.*, *Rev. Sci. Instrum.* **67**, 1120 (1996).
- <sup>2</sup>M. Reiser, *Theory and Design of Charged Particle Beams* (Wiley VCH, Weinheim, 2008).
- <sup>3</sup>M. D. Gabovich, *Usp. Fiz. Nauk* **121**, 259–284 (1977) and references therein.
- <sup>4</sup>A. J. T. Holmes, *Phys. Rev. A* **19**, 389 (1979).
- <sup>5</sup>I. Brown, *The Physics and Technology of Ion Sources*, 1st ed. (Wiley, NY, 1989), Chap. 4 and references therein.
- <sup>6</sup>I. A. Soloshenko, *Rev. Sci. Instrum.* **75**, 1694 (2004) and references therein.
- <sup>7</sup>J. D. Sherman, P. V. Allison, and H. V. Smith, *IEEE Trans. Nucl. Sci.* **32**, 1973 (1985).
- <sup>8</sup>J. D. Sherman, E. Pitcher, and P. V. Allison, in *Proceedings of 1988 Linear Accelerator Conference*, Virginia, USA, Williamsburg, 1988.

- <sup>9</sup>M. Cavenago, G. Serianni, C. Baltador, M. Barbisan, M. De Muri *et al.*, *Fusion Eng. Des.* **146**, 749–752 (2019).
- <sup>10</sup>M. A. Lieberman and A. J. Lichtenberg, *Principles of Plasma Discharges and Materials Processing* (John Wiley & Sons, Inc., Hoboken, New Jersey, 2005).
- <sup>11</sup>O. Auciello, D. L. Flamm, and N. Hershkowitz, *Plasma-Materials Interactions* (Academic Press, Inc., San Diego, 1989), Vol. 1, Chap. 3.
- <sup>12</sup>E. Sartori, A. Pimazzoni, P. Veltri, M. Cavenago, and G. Serianni, *AIP Conf. Proc.* **2052**, 070002 (2018).
- <sup>13</sup>E. Sartori, T. J. Maceina, P. Veltri, M. Cavenago, and G. Serianni, *Rev. Sci. Instrum.* **87**, 02B917 (2016).
- <sup>14</sup>J. Bredin, P. Chabert, and A. Aanesland, *Phys. Plasmas* **21**, 123502 (2014).
- <sup>15</sup>H. Amemiya, B. M. Annaratone, and J. E. Allen, *J. Plasma Phys.* **60**(1), 81–93 (1998).